Development of nanocomposite collagen/ HA/β-TCP scaffolds with tailored gradient porosity and permeability using vitamin E

Mehdi Ebrahimi [1*], Michael Botelho [1*], William Lu [2], Naruporn Monmaturapoj [3]

[1] Restorative Dental Sciences, Prince Philip Dental Hospital, The University of Hong Kong, Hong Kong
[2] Orthopaedics and Traumatology, Li Ka Shing Faculty of Medicine, The University of Hong Kong, Hong Kong
[3] National Metal and Materials Technology Center (MTEC), NSTDA, Thailand

*Corresponding author: ebrahimi@connect.hku.hk, Prince Philip Dental Hospital, 34 hospital road, Sai Ying Pun, Hong Kong

Abstract

The production of the biomimetic scaffolds with well-designed porosity parameters is a critical and challenging factor in biomaterials processing. The porosity parameters (i.e., pore size, pore shape, and distribution pattern) impact scaffold permeability, proteins/cells infiltration, and angiogenesis. This study introduced a new approach for the production of gradient porous nanocomposite scaffolds with controllable porosity and permeability using basic biomaterials of collagen and nano biphasic calcium phosphate (nBCP) powder consisting of nano HA/β-TCP. A modified freeze-drying method (i.e., variables; collagen/nBCP ratio and quenching rates) was integrated for the first time with the chemical foaming method with the use of vitamin E as a potential surfactant and porogen. Vitamin E successfully increased the range of pore size, pore interconnection, and scaffold permeability. Further control of collagen/nBCP ratios and quenching rates allowed modulation of the pore morphology, total porosity, and the surface roughness of the scaffold. Scaffolds produced using vitamin E with collagen/nBCP ratio of 92/8% at -80 ℃ quenching rate displayed a multimodal heterogeneous pore network with a wide range of pore sizes of mostly round/oval and polygonal pore morphology. Furthermore, these scaffolds revealed a more consistent gradient porous network with peripheral large pores – that gradually become smaller toward scaffold central – that produced a significantly higher permeability and better support of initial cellular performances. Accordingly, considering the various potentials of vitamin E, this study would provide promising insight into the production of smart and customized scaffolds for regenerative and therapeutic applications.

Keywords: Vitamin E, Freeze-drying, gradient porosity, permeability, nanocomposite scaffold

This article has been accepted for publication and undergone full peer review but has not been through the copyediting, typesetting, pagination and proofreading process which may lead to differences between this version and the Version of Record. Please cite this article as doi: 10.1002/jbm.a.36990

1. INTRODUCTION

Natural bone is a functionally gradient structure organized in a way that porosity and subsequently the mechanical property vary from its peripheral to central regions. The peripheral cortical region of bone demonstrates very low porosity (5-10%) which gradually increases toward the central region (50-90%) [(1),(2)]. Such architecture renders the bone a non-uniform gradient porous structure which is also seen in other tissues such as cartilage and skin [(3),(4)].

Considering the biomimetic strategies, it is generally recommended to expand the range of pore size similar to the natural bone that exhibits a wide range of pore sizes based on the physiological requirements [(5),(6)]. This is reported to support signaling molecules interaction and nutrition/waste transport (nanopores), cell attachment and migration and capillary formation (micropores), and innervations and vascularization (macropores) [(7)–(9)].

Moreover, further control of the porosity distribution is required during the production of the biomimetic bone scaffold with a gradient porosity pattern. This porosity pattern is reported to modulate cell migration, influence cell differentiation, and improve osteogenic differentiation of stem cells [(10)]. It is also assumed to increase the scaffold permeability and hydrophilicity [(11),(12)] that in turn enhances cellular infiltration and angiogenesis [(9),(13)]. Moreover, it can offer an ideal environment for basic cell studies, repair of composite tissues, and guided tissue regeneration [(9)]. Unfortunately, the clinical examples of such scaffolds are rare due to manufacturing cost and design complexity.

Ideally, considering the impact of porosity parameters (i.e., pore size, pore shape, and distribution pattern) on the bioactivity of the scaffold [(9),(14)], a manufacturing method is required to allow the development of non-uniform, heterogeneous, multimodal porous scaffold with high pore interconnectivity and a range of controllable porosity parameters

rather than single size and pattern [15]. For this purpose, different techniques have been proposed, e.g., unidirectional solidification, freeze-drying, solvent casting, particulate/porogen leaching, gas foaming, and additive manufacturing technologies (CAD/CAM) [16]–[18]. However, the available techniques suffer from limited control over porosity parameters, inadequate pore interconnectivity and permeability, high cost, high processing temperature, limited resolution, and use of toxic solvents [17],[19].

The freeze-drying technique has received considerable attention because of its ability to produce high porosity and interconnectivity at low temperatures [20]. Furthermore, it is a simple and safe method for preserving the original structure of thermo-sensitive polymers (e.g., collagen) during material processing [20]. However, the overall procedure is time-consuming and offers limited control over porosity [20]. Therefore, different modifications have been suggested to overcome these limitations such as; addition of different surfactants (i.e., polyvinyl alcohol and polyethylene glycol) and porogens (e.g., NaCl) [21]. However, there are ongoing challenges such as improper control of porosity and the cytotoxic potentials of remnant additives in the final products [21].

D-α-Tocopheryl Polyethylene Glycol 1000 Succinate (TPGS) with an empirical formula of $C_{33}O_5H_{54}(CH_2CH_2O)_n$ is a water-soluble derivative and the most active isoform of vitamin E [22]. TPGS is a safe FDA-approved chemical agent that is primarily known because of its antioxidant properties. TPGS various applications as plasticizer [23], anticancer [24], bioavailability enhancer [25], and drug carrier [26] have been documented. However, this study accurately analyzed for the first time the ability of TPGS as a potential surfactant/porogen in the production of a well-controlled porous nanocomposite scaffold for non-load bearing applications.

2. MATERIALS AND METHODS

2.1. Scaffolds preparation

Biphasic calcium phosphate nanoparticle (nBCP) was produced in our lab as described previously [27],[28]. Briefly, a controlled calcining temperature of 900 ℃ was implemented during a modified wet mechano-chemical method to produce calcium-deficient carbonate-substituted nanoparticles (nHA/nβ-TCP%: 92/8%) with high crystallinity (~100%) and

homogeneity, 58 nm particle size, and 1.83 Ca/P molar ratio. A commercial type of pure collagen solution was purchased (atelocollagen sol 1% w/v, KIWAKI, Japan) to prepare three groups of nanocomposite scaffolds; study (collagen/nBCP with TPGS), control (collagen/nBCP without TPGS), and standard (pure collagen). The slurry was prepared at room temperature by mechanical mixing using an electric stirrer in two different composition ratios of collagen/nBCP; 85/15, and 92/8 weight %. Later, the TPGS (Sigma, 20% weight % in DI) was added stepwise to the slurry in two different weight %; 5% and 15%. The selected ratios of collagen/nBCP and TPGS were based on the pilot studies according to their processability, manipulability and best physical performances. Then, the slurry was poured into cylindrical custom-made molds (∅11x15 mm) and exposed to two selected quenching rates; -80 °C (deep freezer for 1 hour; D rate) and -18 °C (conventional freezer for 12 hours; F rate). The selected quenching rates were based on the pilot studies in our lab. Later, samples were freeze-dried at -80 °C and 0.06 mbar vacuum pressures (ThermoFisher Scientific, US) for 36-48 hours. Finally, the scaffolds were stabilized by immersion in a chemical crosslinker solution of *N*-(3-Dimethylaminopropyl)-*N′*-ethylcarbodiimide hydrochloride (EDC, Sigma) combined with N-hydroxysuccinimide (NHS, Sigma) (EDC/NHS: 50mM/25mM) in 98% ethanol for 4 hours [29]. This was followed by a washing phase (0.1 M of Na_2HPO_4) and plasma sterilization (temperature range of 37- 44 ℃ with 50 min cycle time) which is suitable for heat and moisture-sensitive materials.

2.2. Basic physicochemical characterization

2.2.1. Crystallography (XRD)

The scaffolds were analyzed by X-ray diffractometer (X'pert PRO, PANalytical, Netherland) using Cu radiation (λ=0.15405 nm) operated at 40 kV and 35 mA in continuous scan mode with step size 0.02° from 10° to 60° (2θ). The XRD spectra were analyzed using JADE software and ICDD standard (JCPDS card no. 09-0432 for pure HA and card no. 09-0169 for pure β-TCP).

2.2.2. FTIR spectrophotometry

The dried scaffold was prepared under a hydraulic pressure (ASTM E1252-98) and Fourier Transform Infrared analysis (FTIR spectrometer, Perkin Elmer, US) was

performed using middle-range infrared over a frequency region of 4000-600 (cm^{-1}) wavenumber at a resolution of 4 cm^{-1}.

2.3. Permeability and porosity analysis

2.3.1. Swelling test

The swelling test was performed to measure the swelling ability of the scaffold and the water uptake potential of the scaffold's pore network. This provides information about the degree of scaffold permeability and hydrophilicity. Scaffolds (n=10) of known volume (Ø10x9 mm length) and weight (W_d) were immersed in phosphate buffer saline (PBS, 5ml, pH=7.4) for 1 hour, 48 hours (day 2), and 120 hours (day 5) at room temperature. The swelling ratio was monitored gravimetrically measuring the water uptake as a function of time as follow:

Swelling ratio (%) = $(W_s - W_d) / W_d \times 100$

2.3.2. Total porosity analysis

The total porosity percentage of scaffolds (n=10) were evaluated by the gravimetric method. Apparent density (ρ_a) determined by measuring the volume (cm^3) using a digital caliper and mass (g) by an electronic balance ($\rho_a = m / v$). The theoretical density (ρ_t) of bulk collagen, nHA and nβ-TCP was considered 1.23, 3.156, 3.07 g/cm^3, respectively [30],[31], to determine the theoretical density of collagen/nBCP scaffolds (1.38 g/cm^3 for 92/8% and 1.51 g/cm^3 for 85/15%). The relative total porosity was determined using the following formula:

Porosity (%) = $1 - (\rho_a / \rho_t) \times 100$

2.3.3. SEM analysis

Scaffolds were sputter-coated under vacuum (JEOL, JFC-1200, Japan) and observed using scanning electron microscopy (JEOL, Field Emission SEM, Japan). Microstructural and topographical analyses of scaffolds were performed by studying porosity parameters including; pore size, pore shape, and pore distribution. Besides, the collagen/nBCP configuration and surface roughness were evaluated.

2.3.4. Micro-CT scan

3D analysis of internal pore architecture and porosimetry of scaffold was performed using X-ray computed microtomography (SkyScan 1172, Belgium). Micro-CT was operated at 59 kV, 100 µA, with a spot size of ≤ 5 µm, and a resolution of 6 µm volume pixel (voxel). Later, the cross-sectional images were reconstructed then the inner microstructure and the regional porosity parameters were analyzed (CTAn software, version 1.16.10) by the selection of five different scan zones including upper $1/5^{th}$ (T1), upper $2/5^{th}$ (T2), middle (M), lower $2/5^{th}$ (B2) and lower $1/5^{th}$ (B1). At each scan zone, an average of 10 subsequent slices has been used to represent different porosity parameters. Study parameters included; closed porosity %, open porosity %, and central and peripheral porosity %. The percentage of open porosity was assumed to reflect the degree of pore interconnection.

2.4. Scaffold bioactivity: in vitro cell culture analysis

Within the limit of this study and based on the physicochemical characterization, scaffolds exposed to D rate were selected for cell culture study using MC3T3-E1 (ATCC) cell line. Early cell passage was inoculated ($3x10^5$ cells/ml) on the surface of pre-wetted scaffolds followed by 3 hours incubation time (in 5% CO_2 at 37 °C and 95% humidity). Later, the proliferating medium of α-MEM (Gibco™) containing 10% FBS (Gibco™) and 1% penicillin-streptomycin (Gibco™) was added to cover the scaffold surfaces. After day 10, the medium was replaced by mineralization medium that was prepared by adding 0.15 mM (50 µg/ml) ascorbic acid (Gibco™), 10 mM β-glycerol phosphate (Sigma) and 100 nM dexamethasone (Sigma). The ability of scaffolds in supporting cell attachment (SEM, day 9), proliferation (Alamar blue®, days 1, 5, and 9), and differentiation (ALP, day 21) were studied.

2.5. Statistical analysis

Statistical analysis was performed using SPSS software (SPSS ver. 24) setting the level of statistical significance at $p < 0.05$. All results were represented in the form of mean ± SD. A comparison between different groups was made using the ANOVA test. Multiple comparison tests with Turkey HSD were done if the variances were homogenous.

3. RESULTS

3.1. Crystallography and functional group analysis

XRD results of nanocomposite collagen/nBCP scaffolds showed defined characteristic peaks consistent with ICDD standard relevant to nHA (JCPDS no. 09-0432) as the primary crystalline phase as well as minor peaks relevant to nβ-TCP (JCPDS no. 09-0169) (Fig. 1). When comparing the XRD pattern of nanocomposite scaffolds with that of pure nBCP phases, a minor decrease in diffraction peaks intensities was detected corresponding to the lower crystallinity (low nBCP ratio) or a higher ratio of collagen. However, variables such as different collagen/nBCP ratios, quenching rates and TPGS ratios had no impact on XRD patterns of scaffolds.

Furthermore, the FTIR analysis of nanocomposite scaffolds confirmed the preservation of both mineral and collagen phases. Typical characteristic absorption bands of nBCP minerals were observed that represented HA + β-TCP nanoparticles (92/8 % composition ratio) with type AB carbonate substitution (Fig. 2). The collagen phase also displayed typical absorption peaks of amide bands of proteins (Amide I, II, III, A, and B) with an α-like helical configuration [32].

The possible impact of TPGS on the chemical nature of the produced scaffold was studied in detail. No effect of TPGS was observed on absorption bands of nBCP phases. Furthermore, the main absorption bands of TPGS (Fig. 2) were not traced in the FTIR pattern of crosslinked scaffolds which indicate that TPGS molecules most probably were eliminated during the washing procedure. However, a mild decrease in amide bands A (both 85/15% and 92/8% groups) and the band I (only in 92/8% group) were detected after the addition of TPGS. These data indicate possible minor interactions between collagen and TPGS molecules without a major impact on collagen molecular configurations.

3.2. Analysis of scaffold permeability by the study of swelling percentage

The permeability of the scaffold was found to be dependent on at least four factors; time factor, collagen ratio, TPGS ratio, and quenching rate (Table 1). There was a general increase in the swelling percentage over time with significant changes seen in pure collagen and 92/8% group at D rate. In general, 92/8% group and those with TPGS showed higher swelling percentage than 85/15% group and those without TPGS.

3.3. Evaluation of total porosity ratio

The data confirmed that the total porosity % could be actively modified by controlling three factors; nBCP ratio, TPGS ratio, and quenching rate. In general, 92/8% group displayed a higher porosity % than 85/15% group (Fig 3). The F quenching rate resulted in the reduction of porosity % in the 92/8% group compared to the D rate. However, the addition of TPGS increased porosity % of the F rate over the D rate.

3.4. Microstructural study of scaffold topography

92/8% group (with higher collagen %) showed higher porosity % and larger pore size, where the pore network was more open and interconnected. However, 92/8% group displayed a smoother surface compared to 85/15% group due to the presence of lower nBCP mineral agglomerates. Furthermore, TPGS caused obvious changes in porosity parameters (i.e., pore size, pore shape, and total porosity %) that in turn modified the surface roughness. Moreover, scaffolds without TPGS mostly displayed elongated/tubular pore shapes with fewer pore interconnections. However, TPGS changed the pore shape into primarily round/oval or polygonal with more distinctive and thinner pore walls and higher pore interconnections (Fig. 4). There was also an obvious emergence of minor pores (< 1 μm) with a remarkable increase in the range of pore size. Notably, TPGS 15% resulted in the transformation of pore shape into predominantly round/oval with an increase in mean pore size in 92/8-15% and loss of distinctive surface topography in 85/15-15%.

The quenching rate was also found to have a significant impact on the porosity parameters which was in turn influenced by collagen/nBCP and TPGS ratio. In general, the average pore size and porosity ratio were reduced by a decrease in quenching rates (F > D). D rate created a higher number of smaller pores yielding a highly rough surface, while the F rate showed the minimum number of larger pores with a smoother surface. Concerning the pore shape, the F rate resulted in the round/oval pore while D rate resulted in roughly round/oval and polygonal pore shape.

High SEM magnifications (Fig. 5) revealed the nBCP mineral phase as agglomerate deposits integrated into the backbone of the collagen network or dispersed

homogeneously throughout the collagen surface. As expected, 92/8% group with a lower nBCP % displayed a lower number of mineral agglomerates and smoother surface. Furthermore, high magnifications revealed the abundance of minor pores in the pore walls and surface of scaffolds treated with TPGS.

3.5. Micro-CT scan analysis of porosity

It was found that the 92/8% group has a higher percentage of open porosity and a lower percentage of closed porosity at both central and peripheral regions compared to 85/15% group, independent of quenching rates. However, the impact of TPGS on porosity parameters varied depending on the collagen/nBCP composition ratio, quenching rate, and the scaffold's region under study.

In general, at the F rate (Table 3), TPGS 5% resulted in a significant increase in open/regional porosity at both scaffold central and perimeter of 92/8% group. However, TPGS 15% resulted in a significant decrease and increase of open/regional porosity ratio in 92/8% (at both scaffold central and perimeter) and 85/15% (only at scaffold perimeter) groups, respectively. Considering the impact of quenching rates, it was concluded that the D rate resulted in a higher ratio of open/regional porosity at both scaffold central and perimeter compared to the F rate.

At D rate (Table 4), TPGS 5% caused a remarkable decrease in open/regional porosity of the scaffold central (both 92/8% and 85/15% groups) and perimeter (only 85/15%). However, TPGS 15% reversed this effect by increasing the open/regional porosity again (except the open porosity ratio at scaffold perimeter of 92/8% group). Furthermore, open/regional porosity percentages were found to be higher in scaffold perimeter than it's central, in particular, in the scaffold with TPGS. This finding was more consistent at TPGS 5% independent of quenching rate and collagen/nBCP ratio ($p < 0.05$).

Furthermore**,** Micro-CT cross-sectional images revealed the presence of parallel pore channels connecting the perimeter to the central scaffold (Fig. 6). These parallel pore channels resulted in a higher total porosity (open pores) at the scaffold periphery compared to scaffold central. These channels were more evident at the D rate and less visible at the F rate. At D rate, addition and increasing TPGS % resulted in a higher

number of parallel pore channels with larger dimensions. However, at F rate, TPGS resulted in a less evident but larger pore channel in 85/15% but a more visible and narrower pore channels in 92/8% group.

3.6. Bioactivity of scaffolds: scaffold-cell interactions

3.6.1. Cell proliferation and ALP assay

Within the limit of this study, D rate scaffolds were used for in vitro studies because of their better physical performances. Results of cell viability assay on scaffolds exposed to D rate confirmed the scaffold biocompatibility and lack of cytotoxicity (Fig. 7). In general, 92/8% group supported a higher cell proliferation rate than 85/15% group. Furthermore, it was observed that scaffolds with TPGS supported significantly higher cell attachment and proliferation rate than scaffolds without TPGS. However, no significant difference was found between TPGS 5% and 15% ratios within the same group, except for 92/8-15% on day 9 which supported significantly higher cell numbers than all other groups. Accordingly, the ALP assay on culture day 21 showed no statistical differences between groups; however, a relatively higher ALP activity was noted in TPGS samples, in particular, 92/8-15%.

3.6.2. Cell morphology, attachment, and distribution pattern

On SEM observation (Fig. 8), cells were characterized by spindle-shaped/polygonal morphology and were attached firmly to the scaffold spreading their cytoplasmic extensions and filopodia. Of particular interest was the ability of osteoblast cells to span the pore by their elongated filopodia as a sign of firm attachment that is also reported elsewhere (Fig. 8B) [(33),(34)].

Among all scaffolds, 92/8-15% showed better cellular support by allowing more extensive cellular extensions and the spread of filopodia. Also, the initial secretion of the extracellular matrix was noted in this group with some extracellular mineralized deposits in the form of calcifying spherical nodules distributed on the scaffold surface (Fig. 9).

4. DISCUSSION

4.1. The interaction between processing variables and porosity/permeability parameters

4.1.1. Impact of TPGS on porosity and permeability

The ability of TPGS in modifying the scaffold porosity and permeability parameters can be explained by its significant surface-active properties and amphiphilic nature with the potential to form micelles at a relatively low critical micelle concentration. Furthermore, TPGS can undergo multiple liquid crystalline phase transformations based on micellar re-arrangement by increasing TPGS concentration [35]. Accordingly, our findings supported the ability of TPGS to generate micelles at basically two main phases; the simple phase (TPGS 5%) with the formation of small micelles and hence minor pores, and, the complex phase (TPGS 15%) with the formation of bubbles and hence larger main pores.

It has been reported that the freeze-dried scaffolds display the typical honeycomb-like porous structure [36] with a monomodal pore size distribution pattern and a mean pore size of 100 to 200 µm (usually oriented tubular pore) with isotropic pore interconnections of < 10 µm [20]. However, the addition of a non-ionic surfactant (e.g., Tween) have been reported to alter this porosity pattern by decreasing the range of pore size from 100 to 200 µm to 1 to 50 µm which results in an overall reduction of porosity and production of a trimodal pore distribution pattern [37]. Similarly, in this study, TPGS reduced the total porosity percentages in D rate and F rate scaffolds. However, TPGS caused an increase in the range of pore size (< 1 to 400 µm) and a change of pore shape into mostly oval/round or polygonal with thinner pore walls and higher pore interconnections. This resulted in the scaffold with a multimodal heterogeneous pore network (Fig. 4 and Fig. 5).

Micro-CT scan analysis of the scaffold inner structure (Fig. 6, Table 2, and Table 3) revealed that TPGS could alter the percentage of closed and open porosity based on its concentration which is in turn influenced by the quenching rate and collagen/nBCP ratio. In fact, TPGS micelle forming capacity may be the reason for increasing the percentage of the closed pore within the D rate scaffold treated with a low TPGS ratio of 5%. This, in turn, resulted in reducing the open/regional porosity percentages at both central and perimeter of scaffolds. However, TPGS 15% was found to reverse this effect by increasing the open and regional porosities. This could be attributed to the excessive formation of interconnected micelles or bubbles inside the composite slurry. On the other hand, the scaffold exposed to the F rate showed different behavior where TPGS 5% and 15% resulted in an increase and decrease in open/regional porosity, respectively. This once again implies the importance of the quenching rate on the internal scaffold porosity.

The influence of TPGS on swelling % or scaffold permeability (Table 1), in particular in 92/8% group is by the literature where the application of other non-ionic surfactants was also reported to improve the wettability and the water uptake of the scaffold [37],[38]. This effect can be attributed mainly to the pore-forming ability of TPGS with the generation of minor pores in the pore wall and scaffold surface which in turn increased the surface area and improved the diffusion rate and scaffold permeability [39],[40]. Another possible contributing factor could be the surfactant potential of TPGS that may increase the hydrophilicity of the scaffold and water uptake capacity. However, FTIR analysis of scaffold before and after the crosslinking indicated the absence of TPGS in the chemical composition of the final scaffold (data in supplementary).

Modification of porosity and permeability could be important when considering the possibility of controlling the uptake/release capacity of medicine, modulating the cellular and biological responses, and optimizing the mechanical properties. However, a careful analysis of changes in the scaffold microstructure is required to evaluate the particular impact of TPGS and other processing variables on modulating the porosity parameters through the introduced technique.

4.1.2. Impact of quenching rate

The quenching rate was also found to have a remarkable impact on the porosity parameters. In fact, the impact of the quenching rate on the porosity, hydrophilicity, and permeability has been reported [41]. In general, a continuous reduction in the average pore size and porosity ratio was noted by a decrease in the quenching rate from -18 ℃ (F rate) to -80 ℃ (D rate) (Fig. 4). In particular, the D rate created a higher number of smaller pores yielding a highly rough surface, while the F rate showed the minimum number of larger pores with a smoother surface. This is by the literature that a high quenching rate allows a lower nucleation rate but a higher growth rate that generates larger solvent crystals and hence larger pore size [42]. On the other hand, a low quenching rate is reported to reduce the afforded time for solvent nucleation and subsequent crystal growth, which results in the generation of smaller pores [41] with a more regular and homogenous pore structure [43]. Concerning the pore shape, the F rate resulted in the round/oval pore while D rate resulted in roughly round/oval and polygonal pore shape (Fig. 4A and 3B).

Nevertheless, the presence of tubular parallel pore networks (Fig. 6) correlates with the direction of heat transfer within the collagen/nBCP slurry during freeze-drying.

4.1.3. Impact of collagen and mineral phases

In agreement with the literature [21],[42],[44],[45], we found that collagen % can play an important role in modifying the porosity parameters and permeability. Higher collagen concentration in 92/8% scaffold resulted in the increase in pore size (Fig. 4 and 5), an increase in open pores and a decrease in closed pores (Table 3), and an increase in total porosity percentage. These changes in porosity parameters caused a significant increase in permeability (Table 1). Furthermore, it is reported that the mineral phase could increase the surface roughness that improves the biological behavior by providing a better and more confirms attachment sites for bone cells [42]. Accordingly, in this study both groups revealed surface roughness, however, the higher mineral phase in 85/15% group resulted in a decrease in pore size, open and total porosity, and permeability (Fig. 3, 4 and 5, Table 2).

4.2. The interaction between porosity/permeability and cellular behaviors

The presentation of multiple cellular extensions and long filopodia in this study (Fig. 8) can be attributed to the higher focal adhesion sites on the scaffolds which were produced by nanoscale biomaterials (i.e., smaller grain and higher specific surface area) with favorable surface topography (i.e., nano to micro porosities) [46]. However, the scaffold with TPGS showed a relative decrease ($p > 0.05$) in cell proliferation rate on culture day 9 compared to day 5 (Fig. 7). This may be explained by cells entering the early differentiation phase due to the favorable scaffold topography in this study (i.e., the increased range of pore size with higher microporosity and hydrophilicity). This is reported to reduce the proliferation rates of cells while inducing earlier and higher vascularization and osteogenic differentiation [47].

With regards to pore size, it should be mentioned that the literature recommends a various range of pore sizes (20 to 1500 µm) for bone regeneration [48]. Furthermore, the majority of the available scaffolding materials have a narrow range of pore size with uniform porosity. However, in agreement with the literature [19], it seems that the increased range

of pore size (< 1 to 400 μm) in this study, as well as the controlled pore distribution (gradient porosity), could provide higher support for cells interaction and tissue regeneration.

There is no consensus in the literature about the ideal pore morphology [48]. For example, for enhanced osteogenic differentiation and bone regeneration various range of pore shapes have been suggested such as; columnar pore [49], radial pore [50], and round pore [51]. However, a closer look into the pore morphology of the natural bone reveals that there are also different ranges of pore shapes. As such, increasing the range of pore shape in a controlled pattern could increase the scaffold potential in supporting various interacting cells, new vessels and deposited tissues. However, different pore morphologies is reported to modulate the deposition and quantity of ECM and not the differentiation of cells [52]. Within the context of this study, the MC3T3 cell lines showed a more preference toward round/oval pore morphology which was seen in D rate scaffold with TPGS.

Considering the pore distribution pattern, the potentials of the gradient porous structure have been already discussed in supporting various cell types and composite tissue regeneration [1],[53]. The novelty of this study lies in the design of the gradient porosity specifically tuned to have a higher porosity ratio and pore size at the outer periphery compared to the inner part while maintaining high pore interconnectivity. Furthermore, the presence of parallel pore channels connecting the scaffold's peripheral and central region could be critical in maintaining the vitality of the regenerating tissues inside the scaffold by securing vascularization and cellular infiltration. This could be an ideal pore distribution pattern and a good candidate for effective tissue engineering.

The permeability of the scaffold is also highly related to protein/cell performances on the surface of the scaffold and further infiltration. Application of higher collagen percentage (92/8% group) and lower quenching rates (D rate and F rate) combined with TPGS resulted in a significantly higher permeability. This is related to the surfactant activity of TPGS and the resulted oval/round pore shape, wider range of pore size, higher pore interconnectivity, and well-controlled pore distribution pattern (gradient porosity with larger pores at the scaffold periphery). This optimized porosity and permeability created a favorable environment that supported better cellular performances (attachment,

proliferation, spread, early osteogenic differentiation) on these scaffolds. Furthermore, the permeability factor could be also useful in the field of controlled drug delivery for therapeutic purposes. The scaffold with different permeability or loading capacity could be loaded with different concentrations of regenerative/therapeutic agents to be released at the target area.

In general, the findings of this study support the literature in that porosity and permeability parameters modify the biological behaviors [54] and cells are positively stimulated by a wide range of pore size [48] with round/oval or polygonal pore morphology [51],[55]. Therefore, according to this study, the higher bioactivity could be related to an increase in the range of pore size, a higher percentage of pore interconnection, and optimizing the pore morphology and distribution pattern. Furthermore, the impact of surface roughness should also be noted in improving the biological behavior by providing a better and more confirm attachment sites for cells [42]. However, the biological findings in this study are related to MC3T3 pre-osteoblast cells which may not be generalized to other cell lines. Furthermore, more accurate biological studies including multiple time points analysis using further *in vitro* and *in vivo* studies are required to explore the exact detail of interaction between porosity and hydrophilicity and biological responses on these scaffolds.

4.3. Properties, potentials, and limitations of the produced scaffolds

Considering the chemical composition (collagen/ HA/β-TCP) of the produced scaffolds, these scaffolds can be compared with some similar available commercial bone graft biomaterials such as; Collagraft **(**Zimmer**)**, Cross.Bone matrix (Biotech Dental), and Mastergraft (Medtronic). However, characteristic physical properties of these scaffolds limit their application to the small bony defects in non-load bearing sites; e.g., tooth extraction socket, periodontal/peri-implant bony defect, and spinal surgery.

The significance of the presented results relies on the fact that these scaffolds can be prepared with the desired porosity/permeability depend on the requirements of the recipient site. Based on our findings we recommend scaffold with oval/round/polygonal

pore morphology with a wide range of pore sizes for further analysis which was better seen in the D rate 92/8% scaffolds produced with TPGS. Furthermore, these scaffolds demonstrated a gradient porous network with a scaffold perimeter of higher porosity connected to the scaffold central of lower porosity by parallel open-pore channels (Fig. 6B). This unique porosity design could provide the following potentials; a) improves the scaffold permeability and facilitates biofluid and cellular infiltration [11],[12], b) avoid over-population of cells on the scaffold surface and prevent the development of necrotic zones inside the scaffold [11], c) promote early and high vascularization of implant bed, therefore, it could be a good candidate for tissue regeneration in the area suffering from poor wound healing or defective vascularization; e.g., infection, diabetic mellitus, *etc*.) [11],[13], d) could allow concurrent growth of different cell types [1], and, e) could be used in the area of drug delivery for loading and controlled release of molecules of different concentration based on the permeability (uptake %) of the scaffold. Finally, considering various clinical advantages of TPGS (e.g., antioxidant, drug carrier potential, bioavailability enhancer, *etc*.), the introduced production method can be further investigated for the development of customized scaffold (i.e., incorporation of signaling/therapeutic agents and stem cells) for various tissue engineering applications (Fig. 10).

5. CONCLUSION

This study demonstrated the potential of a simple and cost-effective method in the production of structurally graded biomimetic bone scaffold using vitamin E (TPGS). The introduced method allowed the development of a well-controlled gradient porous scaffold with a multimodal heterogeneous pore network and a wide range of pore size with round/oval/polygonal pore morphology. The novelty of this paper relies on the use of vitamin E as an active porogen and surfactant to optimize the porosity and increase the permeability of the scaffold. Considering the potential of vitamin E (TPGS), this method can be a promising one for further research and production of customized or smart scaffolding biomaterials for bone tissue engineering and other regenerative and therapeutic applications.

Disclosures

The authors declare that they have no competing interests.

Acknowledgment

The authors would like to acknowledge seed funding for basic research (HKU, Hong Kong) and project grant of MTEC/NSTDA (Thailand) for their kind support.

REFERENCES

1. Miao X, Sun D. Graded/Gradient Porous Biomaterials. Materials (Basel) [Internet]. 2009;3:26–47. Available from: http://www.mdpi.com/1996-1944/3/1/26
2. Cooper DML, Kawalilak CE, Harrison K, Johnston BD, Johnston JD. Cortical Bone Porosity: What Is It, Why Is It Important, and How Can We Detect It? Curr Osteoporos Rep [Internet]. 2016;14:187–98. Available from: http://link.springer.com/10.1007/s11914-016-0319-y
3. Zhu Y, Wu H, Sun S, Zhou T, Wu J, Wan Y. Designed composites for mimicking compressive mechanical properties of articular cartilage matrix. J Mech Behav Biomed Mater [Internet]. 2014;36:32–46. Available from: http://www.ncbi.nlm.nih.gov/pubmed/24793172
4. Rahmati M, Blaker JJ, Lyngstadaas SP, Mano JF, Haugen HJ. Designing multigradient biomaterials for skin regeneration. Mater Today Adv [Internet]. 2020;5:100051. Available from: https://linkinghub.elsevier.com/retrieve/pii/S2590049819301250
5. Murphy CM, Haugh MG, O'Brien FJ. The effect of mean pore size on cell attachment, proliferation and migration in collagen-glycosaminoglycan scaffolds for bone tissue engineering. Biomaterials. 2010;31:461–6.
6. Haugh MG, Murphy CM, O'Brien FJ. Novel freeze-drying methods to produce a range of collagen-glycosaminoglycan scaffolds with tailored mean pore sizes. Tissue Eng Part C Methods [Internet]. 2010;16:887–94. Available from: http://www.ncbi.nlm.nih.gov/pubmed/19903089
7. Oh SH, Park IK, Kim JM, Lee JH. In vitro and in vivo characteristics of PCL scaffolds with pore size gradient fabricated by a centrifugation method. Biomaterials [Internet]. 2007;28:1664–71. Available from: http://www.ncbi.nlm.nih.gov/pubmed/17196648
8. Ouyang P, Dong H, He X, Cai X, Wang Y, Li J, Li H, Jin Z. Hydromechanical mechanism behind the effect of pore size of porous titanium scaffolds on osteoblast response and bone ingrowth. Mater Des [Internet]. 2019;183:108151. Available from: https://linkinghub.elsevier.com/retrieve/pii/S0264127519305891
9. Loh QL, Choong C. Three-dimensional scaffolds for tissue engineering applications: role of porosity and pore size. Tissue Eng Part B Rev. 2013;19:485–502.
10. Di Luca A, Ostrowska B, Lorenzo-Moldero I, Lepedda A, Swieszkowski W, Van Blitterswijk C, Moroni L. Gradients in pore size enhance the osteogenic differentiation of human mesenchymal stromal cells in three-dimensional scaffolds. Sci Rep [Internet]. 2016;6:22898. Available from: http://www.nature.com/articles/srep22898
11. Mitsak AG, Kemppainen JM, Harris MT, Hollister SJ. Effect of polycaprolactone scaffold permeability on bone regeneration in vivo. Tissue Eng Part A [Internet]. 2011;17:1831–9. Available from: http://www.ncbi.nlm.nih.gov/pubmed/21395465
12. Emans PJ, Jansen EJP, van Iersel D, Welting TJM, Woodfield TBF, Bulstra SK, Riesle J, van Rhijn LW, Kuijer R. Tissue-engineered constructs: the effect of scaffold architecture in osteochondral repair. J Tissue Eng Regen Med [Internet]. 2013;7:751–6. Available from: http://www.ncbi.nlm.nih.gov/pubmed/22438217
13. Causa F, Netti PA, Ambrosio L. A multi-functional scaffold for tissue regeneration: the need to engineer a tissue analogue. Biomaterials [Internet]. 2007;28:5093–9. Available from: http://www.ncbi.nlm.nih.gov/pubmed/17675151
14. Rasoulianboroujeni M, Yazdimamaghani M, Khoshkenar P, Pothineni VR, Kim KM, Murray TA, Rajadas J, Mills DK, Vashaee D, Moharamzadeh K, Tayebi L. From solvent-

free microspheres to bioactive gradient scaffolds. Nanomedicine Nanotechnology, Biol Med. 2017;13:1157–69.
15. Mansouri N, SamiraBagheri. The influence of topography on tissue engineering perspective. Mater Sci Eng C [Internet]. 2016;61:906–21. Available from: http://linkinghub.elsevier.com/retrieve/pii/S0928493115307050
16. Sobral JM, Caridade SG, Sousa RA, Mano JF, Reis RL. Three-dimensional plotted scaffolds with controlled pore size gradients: Effect of scaffold geometry on mechanical performance and cell seeding efficiency. Acta Biomater [Internet]. 2011;7:1009–18. Available from: http://www.ncbi.nlm.nih.gov/pubmed/21056125
17. Zhou T, Wu J, Liu J, Luo Y, Wan Y. Fabrication and characterization of layered chitosan/silk fibroin/nano-hydroxyapatite scaffolds with designed composition and mechanical properties. Biomed Mater [Internet]. 2015;10:045013. Available from: http://www.ncbi.nlm.nih.gov/pubmed/26225911
18. Bandyopadhyay A, Espana F, Balla VK, Bose S, Ohgami Y, Davies NM. Influence of porosity on mechanical properties and in vivo response of Ti6Al4V implants. Acta Biomater. 2010;6:1640–8.
19. Bidan CM, Kommareddy KP, Rumpler M, Kollmannsberger P, Fratzl P, Dunlop JWC. Geometry as a Factor for Tissue Growth: Towards Shape Optimization of Tissue Engineering Scaffolds. Adv Healthc Mater [Internet]. 2013;2:186–94. Available from: http://doi.wiley.com/10.1002/adhm.201200159
20. Collins MN, Birkinshaw C. Hyaluronic acid based scaffolds for tissue engineering--a review. Carbohydr Polym [Internet]. 2013;92:1262–79. Available from: http://www.ncbi.nlm.nih.gov/pubmed/23399155
21. Akbarzadeh R, Yousefi A-M. Effects of processing parameters in thermally induced phase separation technique on porous architecture of scaffolds for bone tissue engineering. J Biomed Mater Res Part B Appl Biomater [Internet]. 2014;102:1304–15. Available from: http://doi.wiley.com/10.1002/jbm.b.33101
22. Wang K, Zhou C, Hong Y, Zhang X. A review of protein adsorption on bioceramics. Interface Focus. 2012;2:259–77.
23. Repka MA, McGinity JW. Influence of vitamin E TPGS on the properties of hydrophilic films produced by hot-melt extrusion. Int J Pharm [Internet]. 2000;202:63–70. Available from: http://www.ncbi.nlm.nih.gov/pubmed/10915927
24. Zhang H, Xu G, Liu T, Xu L, Zhou Y. Foam and interfacial properties of Tween 20–bovine serum albumin systems. Colloids Surfaces A Physicochem Eng Asp [Internet]. 2013;416:23–31. Available from: http://linkinghub.elsevier.com/retrieve/pii/S0927775712007054
25. Cianetti S, Cooper VB, Attenni B, Pucci V, Fiore F, Giuliano C, Laufer R, Gardelli C, Monteagudo E, Narjes F, Pearce GE, Rowley M. Enhancement of intestinal absorption of 2-methyl cytidine prodrugs. Drug Deliv [Internet]. 2010;17:214–22. Available from: http://www.ncbi.nlm.nih.gov/pubmed/20233089
26. di Cagno M, Stein PC, Styskala J, Hlaváč J, Skalko-Basnet N, Bauer-Brandl A. Overcoming instability and low solubility of new cytostatic compounds: a comparison of two approaches. Eur J Pharm Biopharm [Internet]. 2012;80:657–62. Available from: http://www.ncbi.nlm.nih.gov/pubmed/22142591
27. Ebrahimi M. Biomimetic principle for development of nanocomposite biomaterials in tissue engineering. Appl Nanocomposite Mater Orthop [Internet]. Elsevier; 2019. Available from: https://linkinghub.elsevier.com/retrieve/pii/B9780128137406000156
28. Ebrahimi M, Botelho M. Adult Stem Cells of Orofacial Origin: Current Knowledge and Limitation and Future Trend in Regenerative Medicine. Tissue Eng Regen Med. 2017;14:719–33.
29. Sionkowska A, Kozłowska J. Properties and modification of porous 3-D collagen/hydroxyapatite composites. Int J Biol Macromol [Internet]. 2013;52:250–9. Available from: http://linkinghub.elsevier.com/retrieve/pii/S0141813012003881

30. Tierney CM, Haugh MG, Liedl J, Mulcahy F, Hayes B, O'Brien FJ. The effects of collagen concentration and crosslink density on the biological, structural and mechanical properties of collagen-GAG scaffolds for bone tissue engineering. J Mech Behav Biomed Mater [Internet]. 2009;2:202–9. Available from: http://www.ncbi.nlm.nih.gov/pubmed/19627824
31. Li S, De Wijn JR, Li J, Layrolle P, De Groot K. Macroporous biphasic calcium phosphate scaffold with high permeability/porosity ratio. Tissue Eng [Internet]. 2003;9:535–48. Available from: http://www.ncbi.nlm.nih.gov/pubmed/12857421
32. Petibois C, Gouspillou G, Wehbe K, Delage J-P, Déléris G. Analysis of type I and IV collagens by FT-IR spectroscopy and imaging for a molecular investigation of skeletal muscle connective tissue. Anal Bioanal Chem [Internet]. 2006;386:1961–6. Available from: http://www.ncbi.nlm.nih.gov/pubmed/17043797
33. Brodie JC, Goldie E, Connel G, Merry J, Grant MH. Osteoblast interactions with calcium phosphate ceramics modified by coating with type I collagen. J Biomed Mater Res A [Internet]. 2005;73:409–21. Available from: http://www.ncbi.nlm.nih.gov/pubmed/15892144
34. Ebrahimi M, Pripatnanont P, Suttapreyasri S, Monmaturapoj N. In vitro biocompatibility analysis of novel nano-biphasic calcium phosphate scaffolds in different composition ratios. J Biomed Mater Res B Appl Biomater. 2014;102:52–61.
35. Shah AR, Banerjee R. Effect of D-α-tocopheryl polyethylene glycol 1000 succinate (TPGS) on surfactant monolayers. Colloids Surf B Biointerfaces [Internet]. 2011;85:116–24. Available from: http://www.ncbi.nlm.nih.gov/pubmed/21398100
36. Román J, Cabañas MV, Peña J, Vallet-Regí M. Control of the pore architecture in three-dimensional hydroxyapatite-reinforced hydrogel scaffolds. Sci Technol Adv Mater [Internet]. 2011;12:045003. Available from: http://www.tandfonline.com/doi/full/10.1088/1468-6996/12/4/045003
37. Marras-Marquez T, Peña J, Veiga-Ochoa MD. Agarose drug delivery systems upgraded by surfactants inclusion: Critical role of the pore architecture. Carbohydr Polym [Internet]. 2014;103:359–68. Available from: http://linkinghub.elsevier.com/retrieve/pii/S014486171301240X
38. Adibkia K, Ghanbarzadeh S, Shokri MH, Arami Z, Arash Z, Shokri J. Micro-porous surfaces in controlled drug delivery systems: design and evaluation of diltiazem hydrochloride controlled porosity osmotic pump using non-ionic surfactants as pore-former. Pharm Dev Technol [Internet]. 2014;19:507–12. Available from: http://www.tandfonline.com/doi/full/10.3109/10837450.2013.805774
39. Naseri N, Poirier J-M, Girandon L, Fröhlich M, Oksman K, Mathew AP. 3-Dimensional porous nanocomposite scaffolds based on cellulose nanofibers for cartilage tissue engineering: tailoring of porosity and mechanical performance. RSC Adv [Internet]. 2016;6:5999–6007. Available from: http://xlink.rsc.org/?DOI=C5RA27246G
40. Sultan S, Mathew AP. 3D printed scaffolds with gradient porosity based on a cellulose nanocrystal hydrogel. Nanoscale [Internet]. 2018;10:4421–31. Available from: http://xlink.rsc.org/?DOI=C7NR08966J
41. Budyanto L, Goh YQ, Ooi CP. Fabrication of porous poly(L-lactide) (PLLA) scaffolds for tissue engineering using liquid-liquid phase separation and freeze extraction. J Mater Sci Mater Med [Internet]. 2009;20:105–11. Available from: http://www.ncbi.nlm.nih.gov/pubmed/18704655
42. Zhang R, Ma PX. Poly(alpha-hydroxyl acids)/hydroxyapatite porous composites for bone-tissue engineering. I. Preparation and morphology. J Biomed Mater Res [Internet]. 1999;44:446–55. Available from: http://www.ncbi.nlm.nih.gov/pubmed/10397949
43. Sun F, Lim B-K, Ryu S-C, Lee D, Lee J. Preparation of multi-layered film of hydroxyapatite and chitosan. Mater Sci Eng C [Internet]. 2010;30:789–94. Available from: http://linkinghub.elsevier.com/retrieve/pii/S092849311000069X
44. Freyman TM, Yannas IV, Gibson LJ. Cellular materials as porous scaffolds for tissue

engineering. Prog Mater Sci [Internet]. 2001;46:273–82. Available from: http://linkinghub.elsevier.com/retrieve/pii/S0079642500000189
45. O'Brien FJ, Harley BA, Yannas I V, Gibson L. Influence of freezing rate on pore structure in freeze-dried collagen-GAG scaffolds. Biomaterials. 2004;25:1077–86.
46. Jin H-B, Guo C-B, Mao K-Y, Dorozhkin S, Agathopoulos S. Preparation of porous biphasic β-TCP/HA bioceramics with a natural trabecular structure from calcined cancellous bovine bone. J Ceram Soc Japan. 2010;118:52–6.
47. Lord MS, Foss M, Besenbacher F. Influence of nanoscale surface topography on protein adsorption and cellular response. Nano Today [Internet]. 2010;5:66–78. Available from: http://linkinghub.elsevier.com/retrieve/pii/S1748013210000058
48. Murphy CM, O'Brien FJ. Understanding the effect of mean pore size on cell activity in collagen-glycosaminoglycan scaffolds. Cell Adh Migr [Internet]. 2010;4:377–81. Available from: http://www.tandfonline.com/doi/abs/10.4161/cam.4.3.11747
49. Liu X, Rahaman MN, Fu Q. Bone regeneration in strong porous bioactive glass (13-93) scaffolds with an oriented microstructure implanted in rat calvarial defects. Acta Biomater [Internet]. 2013;9:4889–98. Available from: http://www.ncbi.nlm.nih.gov/pubmed/22922251
50. Brouwer KM, Daamen WF, van Lochem N, Reijnen D, Wijnen RMH, van Kuppevelt TH. Construction and in vivo evaluation of a dual layered collagenous scaffold with a radial pore structure for repair of the diaphragm. Acta Biomater [Internet]. 2013;9:6844–51. Available from: http://www.ncbi.nlm.nih.gov/pubmed/23499986
51. Sanzana ES, Navarro M, Ginebra M-P, Planell JA, Ojeda AC, Montecinos HA. Role of porosity and pore architecture in the in vivo bone regeneration capacity of biodegradable glass scaffolds. J Biomed Mater Res A [Internet]. 2014;102:1767–73. Available from: http://www.ncbi.nlm.nih.gov/pubmed/23813739
52. Di Luca A, Szlazak K, Lorenzo-Moldero I, Ghebes CA, Lepedda A, Swieszkowski W, Van Blitterswijk C, Moroni L. Influencing chondrogenic differentiation of human mesenchymal stromal cells in scaffolds displaying a structural gradient in pore size. Acta Biomater [Internet]. 2016;36:210–9. Available from: http://linkinghub.elsevier.com/retrieve/pii/S1742706116300988
53. Woodfield TBF, Van Blitterswijk CA, De Wijn J, Sims TJ, Hollander AP, Riesle J. Polymer scaffolds fabricated with pore-size gradients as a model for studying the zonal organization within tissue-engineered cartilage constructs. Tissue Eng [Internet]. 2005;11:1297–311. Available from: http://www.ncbi.nlm.nih.gov/pubmed/16259586
54. Martins RP, Finan JD, Guilak F, Lee DA. Mechanical regulation of nuclear structure and function. Annu Rev Biomed Eng [Internet]. 2012;14:431–55. Available from: http://www.ncbi.nlm.nih.gov/pubmed/22655599
55. Phadke A, Hwang Y, Kim SHSHSH, Kim SHSHSH, Yamaguchi T, Masuda K, Varghese S. Effect of scaffold microarchitecture on osteogenic differentiation of human mesenchymal stem cells. Eur Cell Mater [Internet]. 2013;25:114–29. Available from: http://www.ncbi.nlm.nih.gov/pubmed/23329467

Figure legend

Fig 1. XRD pattern of nanocomposite scaffolds with different TPGS ratios showing the relevant major peaks of nHA (marked with 'v') and nβ-TCP (marked with '*').

Fig. 2. FTIR pattern of pure nBCP, collagen, TPGS, and nanocomposite scaffolds (D rate). For pure collagen, the amide bands are marked. For nBCP the main bands corresponding to the chemical groups are numbered as follows: 1) OH^-, 2) CO_3^{2-}, 3) PO_4^{3-}, and, 4) HPO_4^{2-}. The main bands of TPGS are indicated with stars.

Fig 3. The total porosity of scaffolds at different quenching rates. "*" indicates significant differences between different quenching rates in the same sample.

Fig. 4. SEM views of scaffolds surface topography at F and D rates.

Fig. 5. SEM high magnification views of 92/8% and 85/15% groups.

Fig. 6. A. Micro-CT scan reconstructed images of the scaffolds at mid-section. B. The longitudinal and cross-sectional view of the scaffold. Top) Multimodal gradient porosity with higher peripheral porosity and lower central porosity. Bottom) tubular parallel pore channels connecting the scaffold periphery to the central region.

Fig. 7. Cell proliferation and ALP assay of scaffolds over the culture period. "*": p-value for the comparison within the figure ($p < 0.05$)

Fig. 8. SEM views of cell morphology and attachment on culture day 9. A) A typical spindle-like cell with extended filopodia. B) Spanning of a pore by elongated filopodia of a cell. C) A cell with a polygonal shape of about 30 µm size with extended filopodia over 100 µm. D) Extracellular mineralized deposits in the form of calcifying spherical nodules.

Fig. 9. SEM views of cellular spread on the scaffolds with the secreted extracellular matrix.

Fig.10. The porogen and surfactant potential of vitamin E as it has been demonstrated in this paper. Other documented potentials of vitamin E as an antioxidant, plasticizer, permeability enhancer, drug carrier, and to overcome multi-drug resistance (MDR) could be integrated with porogen/surfactant properties for the production of smart or customized biomaterials in therapeutic and regenerative medicine.

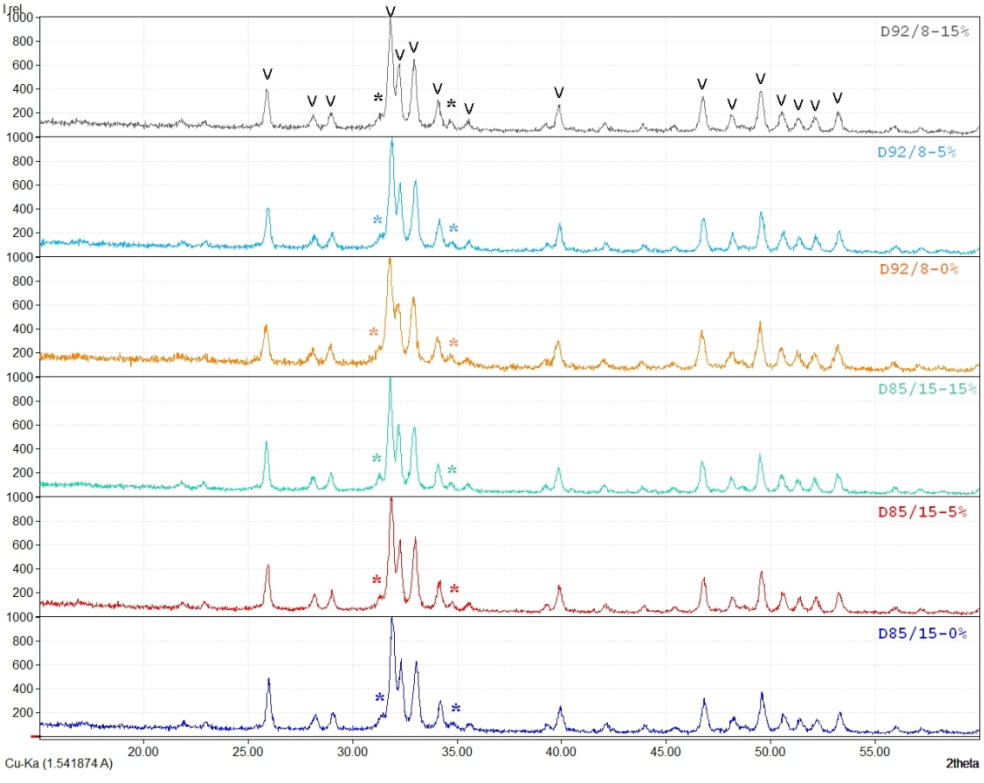

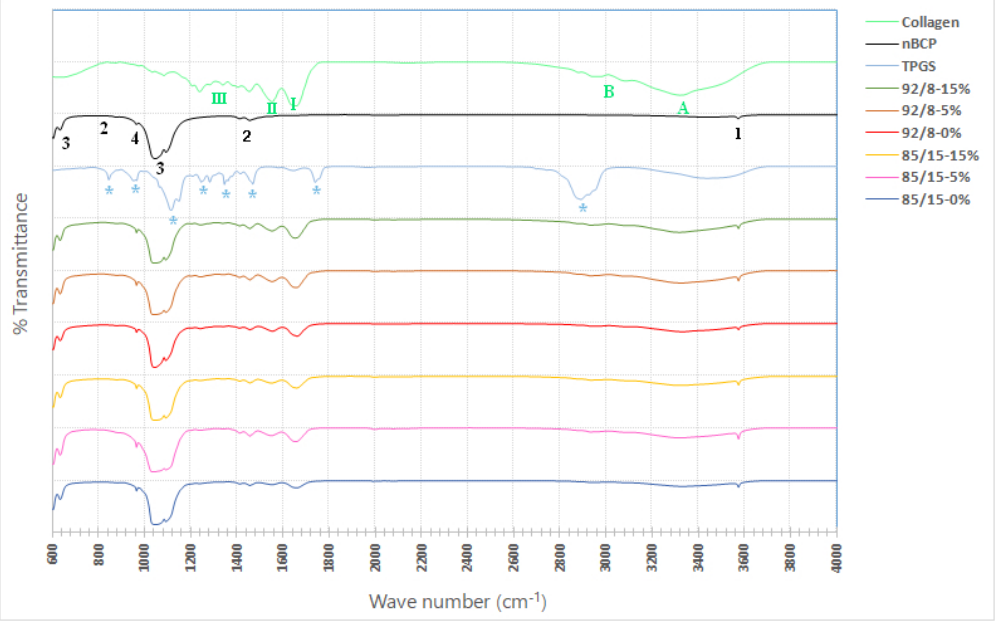

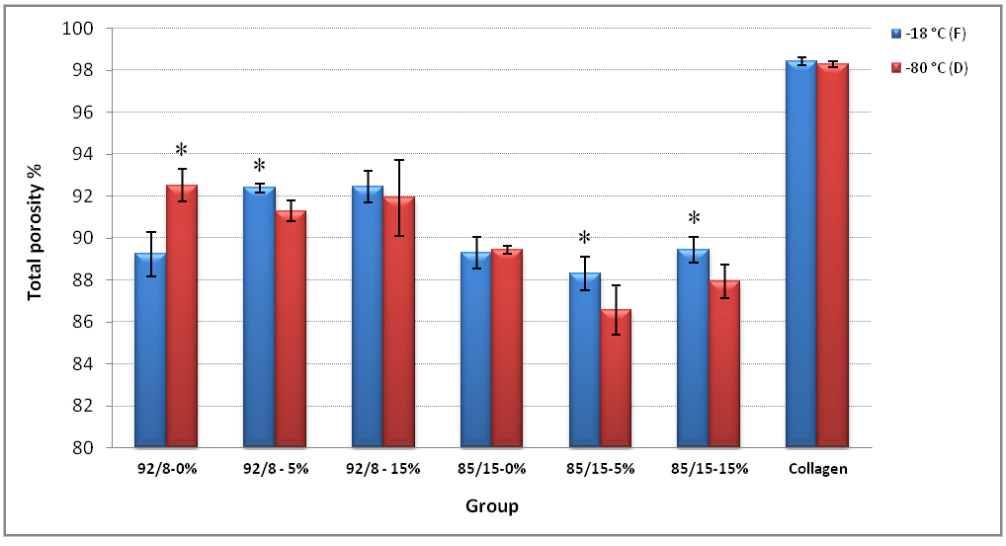

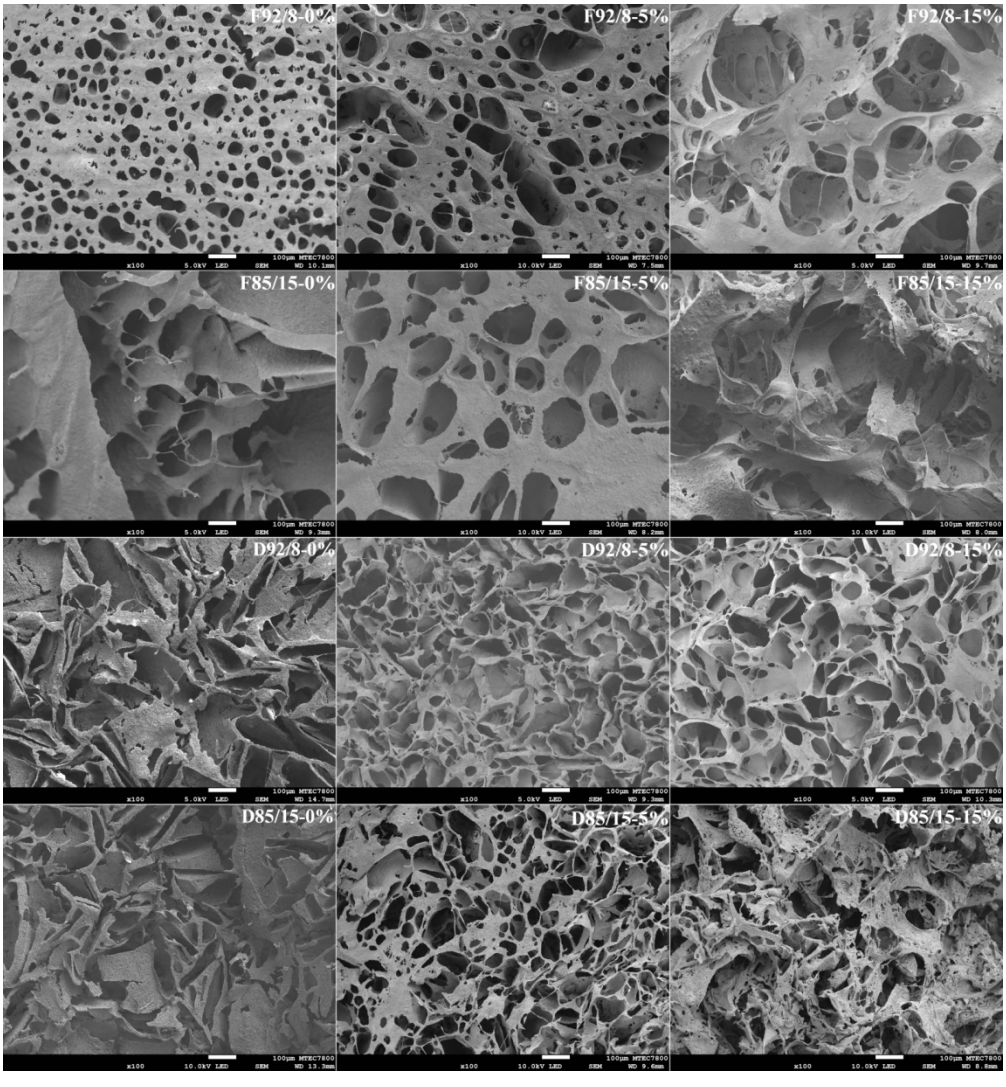

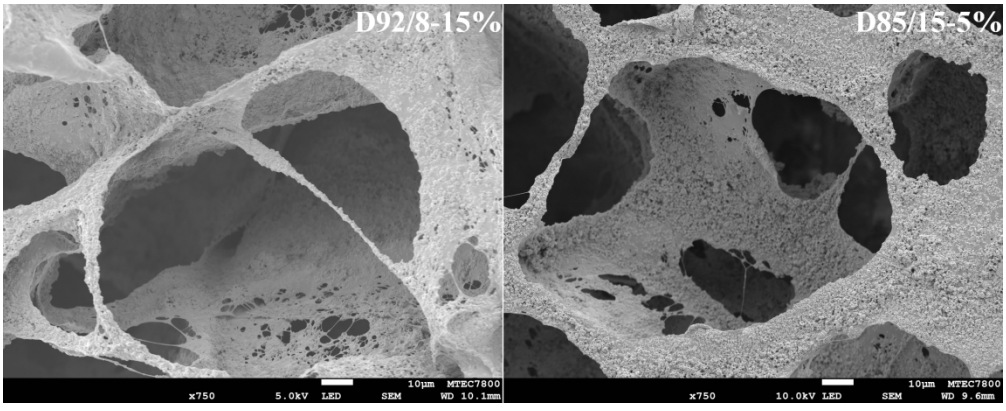

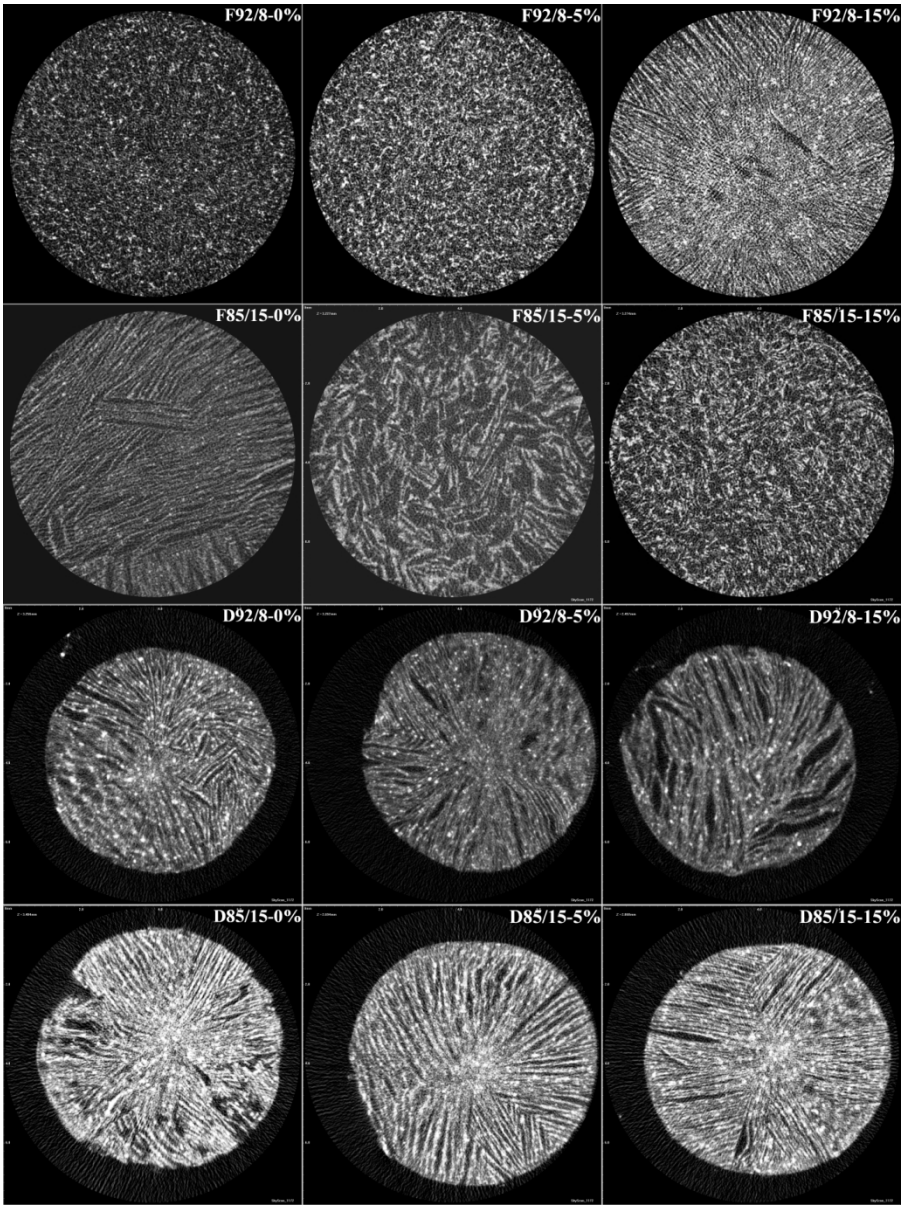

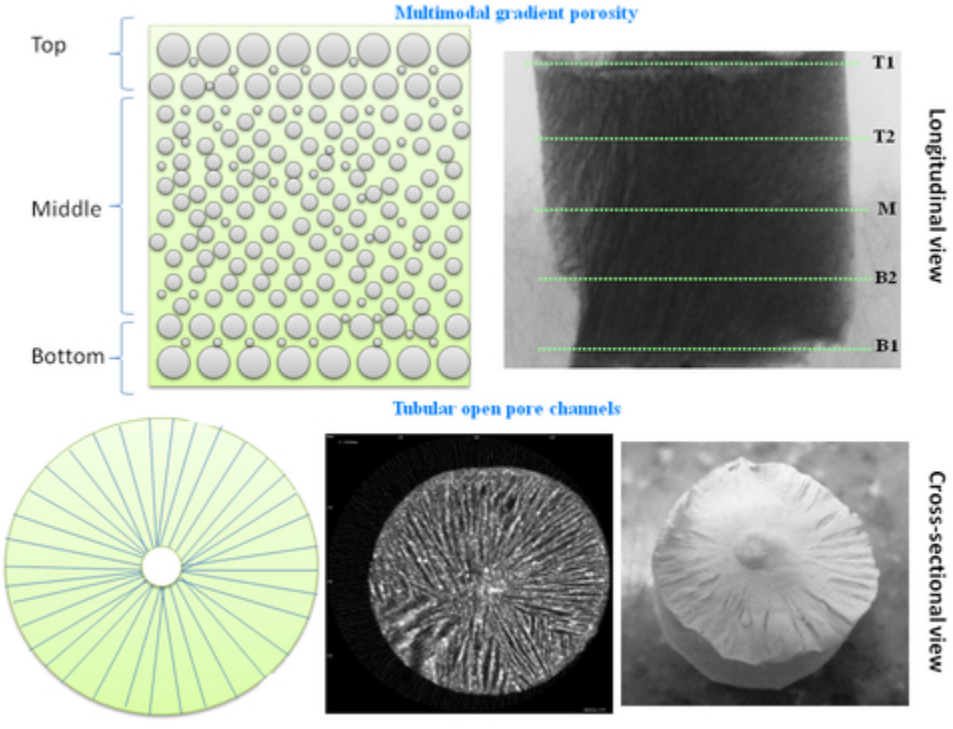

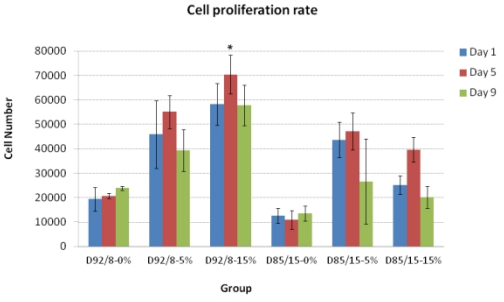

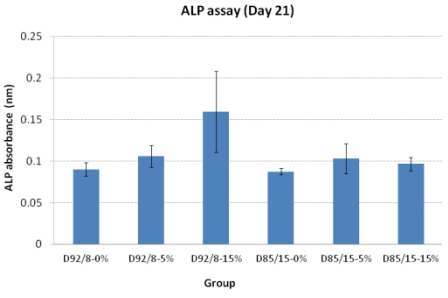

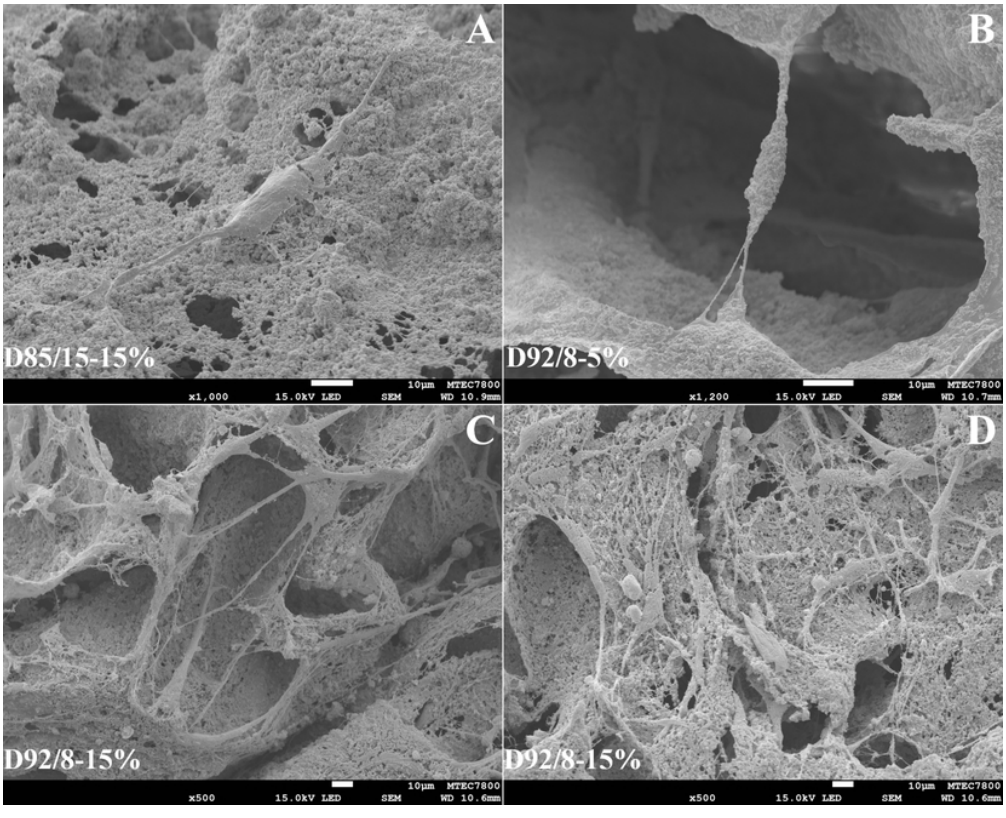

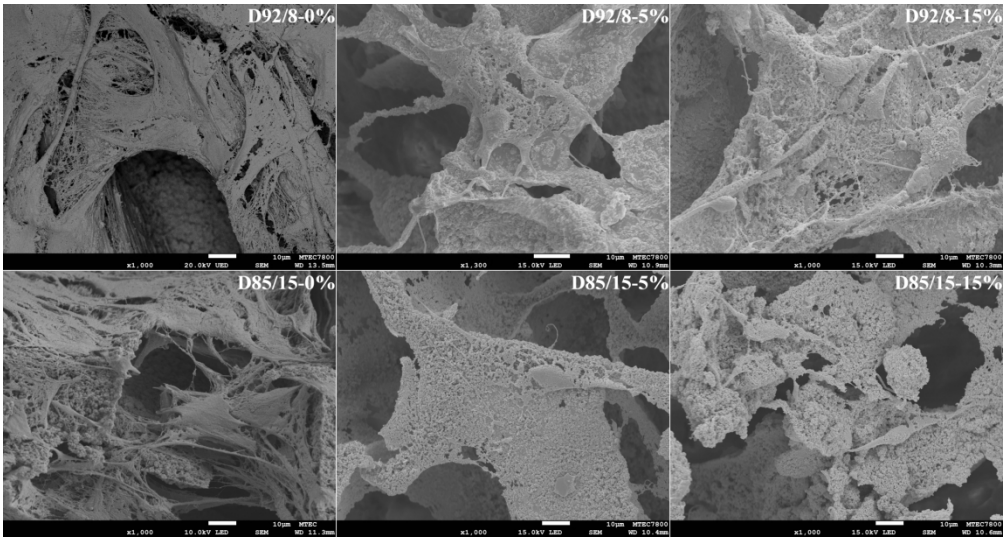

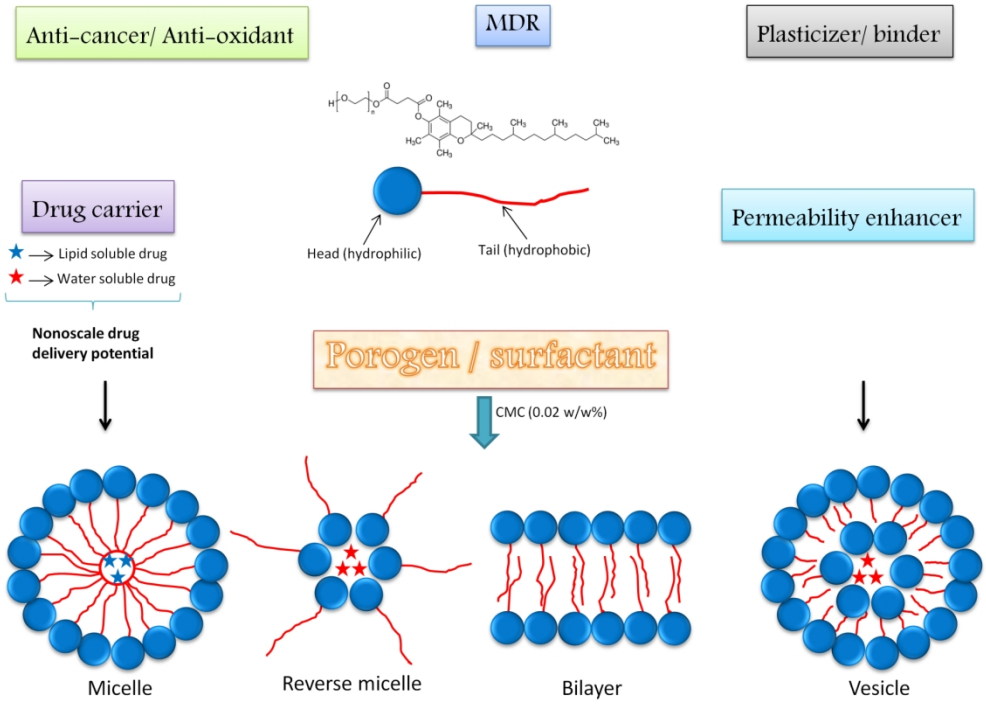

Table 1. Swelling percentage of the scaffolds at different quenching rates over the test period. "*", "#", and "$": the p-value for each comparison within the table. "*" significant differences between quenching rates in the same scaffold/testing time. "#" significant differences between testing times in the same scaffold/quenching rate. "$" significant differences between scaffolds in the same testing time/quenching rate.

Swelling %	**Hour 1**		**Day 2**		**Day 5**	
Group	**-18 °C (F)**	**-80 °C (D)**	**-18 °C (F)**	**-80 °C (D)**	**-18 °C (F)**	**-80 °C (D)**
92/8-0%	712	$758^{\$}$	751	$775^{\#}$	783	$812^{\$\#}$
92/8-5%	$1017^{\$}$	$813^{\$\#}$	$1055^{\$}$	$889^{\$\#}$	$1084^{\$}$	$918^{\$\#}$
92/8-15%	$804^{\$}$	$858^{\$}$	$892^{\$}$	$952^{\$\#}$	$924^{\$}$	$962^{\$\#}$
85/15-0%	$473^{\$}$	489	491	498	505	502
85/15-5%	507	528	532	528	550	538
85/15-15%	552	543	561	555	585	566
Collagen	$2537^{\$\#}$	$3386^{\$\#}$	$3141^{\$\#}$	$3657^{\$\#}$	$3787^{\$\#}$	$3880^{\$\#}$

Table 2: Descriptive table of Fig. 4 explaining the detailed changes in the porosity parameters. It should be noted that the appearance of minor pores increased the range of pore sizes and percentage of pore interconnections. (Pore size range (SR), minor pore (MP), pore shape (S)).

Groups	-18 °C (F)		-80 °C (D)	
	92/8%	85/15%	92/8%	85/15%
0%	S: round SR: 5-100 µm MP: rare	S: irregular SR: 40-150 µm MP: absent	S: tubular SR: 50-400 µm MP: rare	S: tubular SR: 50-300 µm MP: absent
5%	S: altered/ round SR: 15-300 µm MP: visible	S: altered/irregular SR: 20-300 µm MP: visible	S: oval/round/ polygonal SR: 5-200 µm MP: visible	S: oval/round/ polygonal SR: 10-200 µm MP: visible
15%	S: altered/ round SR: 15-400 µm MP: clearly visible	S: completely altered SR: 50-300 MP: clearly visible	S: oval/round SR: 5-250 µm MP: clearly visible	S: irregular SR: 10-250 µm MP: clearly visible

Table 3. F rate: Micro-CT data of porosity parameters at the scaffold's central and peripheral regions. "*" and "$": the p-value for each comparison within the table. "*" significant difference between the ratio of the same group, "$" significant difference between scaffold's central and peripheral regions.

-18 °C (F rate)	**Scaffold perimeter**			**Scaffold central**		
Scaffold	**Closed porosity %**	**Open porosity %**	**Regional porosity %**	**Closed porosity %**	**Open porosity %**	**Regional porosity %**
92/8-0%	15.56±0.71$^{\$}$	84.43±0.71$^{\$}$	95.03±0.35$^{\$}$	28.12±0.24	71.87±0.24	89.68±0.11
92/8-5%	11.46±5.53$^{*\$}$	88.53±5.53$^{*\$}$	96.58±1.82$^{\$}$	19.25±0.15*	80.74±0.151*	93.64±0.05*
92/8-15%	21.98±6.00$^{*\$}$	78.01±6.00$^{*\$}$	92.07±3.05$^{*\$}$	40.04±0.25*	59.95±0.25*	83.75±0.07*
85/15-0%	19.76±6.32$^{\$}$	80.23±6.32	87.17±4.08	21.30±0.40	78.69±0.40	88.19±0.09
85/15-5%	19.18±6.05	80.81±6.05$^{\$}$	88.36±4.21$^{\$}$	25.98±0.44*	74.01±0.44	83.94±0.11
85/15-15%	15.60±12.26$^{*\$}$	84.39±12.26$^{*\$}$	89.20±8.34	21.10±0.30	78.89±0.30	88.079±0.05
Collagen	22.70±0.16	77.29±0.16	93.68±0.032	24.47±1.15	75.52±1.15	93.32±0.03

Table 4. D rate: Micro-CT data of porosity parameters at the scaffold's central and peripheral regions. "*" and "$": the p-value for each comparison within the table. "*" significant difference between the ratio of the same group, "$" significant difference between scaffold's central and peripheral regions.

-80 °C (D rate)	**Scaffold perimeter**			**Scaffold central**		
Scaffold	**Closed porosity %**	**Open porosity %**	**Regional porosity %**	**Closed porosity %**	**Open porosity %**	**Regional porosity %**
92/8-0%	11.96±5.40	88.03±5.40	95.85±1.86	13.52±0.16	86.47±0.16	95.72±0.02
92/8-5%	12.56±7.05$	87.43±7.05$	95.22±2.18$	19.71±0.34*	80.28±0.34*	90.00±0.03*
92/8-15%	15.23±4.15*	84.76±4.15*	94.80±1.89	16.73±0.42	83.26±0.42	93.97±0.01
85/15-0%	20.45±1.69$	79.54±1.69$	91.43±1.81$	24.32±0.06	75.67±0.06	89.31±0.05
85/15-5%	25.71±3.44*$	74.28±3.44*$	88.24±1.95*$	30.18±0.14*	69.81±0.14*	85.29±0.11*
85/15-15%	24.13±5.80*$	75.86±5.80*$	89.19±3.85*$	29.64±0.06	70.35±0.06	86.16±0.04*
Collagen	7.64±5.79	92.35±5.79	96.59±1.86	9.09±0.72	90.90±0.72	95.79±0.20